Journal of Medicinal Chemistry

Article

pubs.acs.org/jmc

Thienopyrimidine Bisphosphonate (ThPBP) Inhibitors of the Human Farnesyl Pyrophosphate Synthase: Optimization and Characterization of the Mode of Inhibition

Chun Yuen Leung,[†] Jaeok Park,[‡] Joris W. De Schutter,[†] Michael Sebag,[⊥] Albert M. Berghuis,[‡,§,†] and Youla S. Tsantrizos*[,∥,‡,†]

[†]Department of Chemistry, McGill University, 801 Sherbrooke Street West, Montreal, Quebec, Canada H3A 0B8

[‡]Department of Biochemistry, McGill University, 3649 Promenade Sir William Osler, Montreal, Quebec, Canada H3G 0B1

[§]Department of Microbiology and Immunology, McGill University, 801 Sherbrooke Street West, Montreal, Quebec, Canada H3A 0B8

[∥]Groupe de Recherche Axé sur la Structure des Protéines, McGill University, 3649 Promenade Sir William Osler, Montreal, Quebec, Canada H3G 0B1

[⊥]Division of Haematology, McGill University Health Center, Royal Victoria Hospital, C6.80, 687 Pine Avenue West, Montreal, Quebec, Canada H3A 1A1

Supporting Information

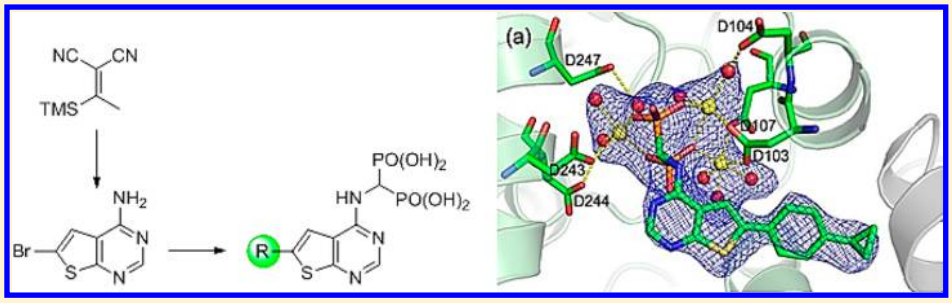

ABSTRACT: Human farnesyl pyrophosphate synthase (hFPPS) controls the post-translational prenylation of small GTPase proteins that are essential for cell signaling, cell proliferation, and osteoclast-mediated bone resorption. Inhibition of hFPPS is a clinically validated mechanism for the treatment of lytic bone diseases, including osteoporosis and cancer related bone metastases. A new series of thienopyrimidine-based bisphosphonates (ThP-BPs) were identified that inhibit hFPPS with low nanomolar potency. Crystallographic evidence revealed binding of ThP-BP inhibitors in the allylic subpocket of hFPPS. Simultaneous binding of inorganic pyrophosphate in the IPP subpocket leads to conformational closing of the active site cavity. The ThP-BP analogues are significantly less hydrophilic yet exhibit higher affinity for the bone mineral hydroxyapatite than the current *N*-BP drug risedronic acid. The antiproliferation properties of a potent ThB-BP analogue was assessed in a multiple myeloma cell line and found to be equipotent to the best current *N*-BP drugs. Consequently, these compounds represent a new structural class of hFPPS inhibitors and a novel scaffold for the development of human therapeutics.

INTRODUCTION

Human farnesyl pyrophosphate synthase (hFPPS) controls the first branching point of the mevalonate pathway and catalyzes the biosynthesis of farnesyl pyrophosphate (FPP). FPP is the key precursor for the biosynthesis of many metabolites, including geranylgeranyl pyrophosphate (GGPP), squalene, and cholesterol. FPP and GGPP are essential for the post-translational prenylation of all small GTPase proteins that play a crucial role in cell signaling, cell proliferation, and osteoclast-mediated bone resorption.[1,2] Inhibition of hFPPS can down-regulate the activity of mutated H-Ras, K-Ras, and N-Ras proteins that function as major drivers of tumor growth in many cancers. For example, whole genome sequencing of human multiple myeloma (MM) tumors has revealed that 50% of MM patients harbored either K-Ras or N-Ras activating mutations, underscoring the importance of hFPPS in this disease.[3] Metastatic bone disease is highly prevalent in patients with MM, breast, and prostate cancers. It is estimated that approximately 70% of all patients with advanced forms of these three types of cancers will at some point develop bone metastases.[4] Thus, the clinical benefits of hFPPS inhibition include both decrease of prenylation of mutated Ras proteins, leading to a decrease in cellular growth and/or survival as well as alleviation of tumor-associated bone destruction via inhibition of osteoclast activity.[5] It is noteworthy that inhibitors

Received: June 25, 2013
Published: September 2, 2013

of the farnesyltransferase enzyme (FTase), which catalyze the prenylation of Ras (e.g., tipifarnib[70]), have also been extensively investigated as an alternative mechanism for downregulating oncogenesis but failed to demonstrate significant clinical efficacy. It was subsequently realized that the substrate specificity of the transferase enzymes (FTase and GGTase I and II) is not absolutely stringent and cross-prenylation can occur, restoring the biological function of the mutated Ras proteins.[71] However, this redundancy mechanism cannot compromise the clinical effects of drugs that *directly* downregulates the biosynthesis of FPP by inhibiting hFPPS.

Additionally, blocking the catalytic activity of hFPPS impacts both the downstream and upstream levels of isoprenoids in the mevalonate pathway, leading to numerous cellular changes. Intracellular accumulation of the substrate isopentenyl pyrophosphate (IPP), as a consequence of hFPPS inhibition, leads to accumulation of an ATP derivative (ApppI), which induces cell apoptosis by inhibiting the mitochondrial adenine nucleotide translocase (ANT).[6,7] IPP is also a natural antigen that directly stimulates $\gamma\delta$ T cells that carry the Vγ2Vδ2 T cell receptors and is strongly implicated in the human innate immune response against tumors.[8] Interestingly, treatment of different types of cancer cells with the same hFPPS inhibitor may result in dramatically different intracellular levels of IPP (from ~10-fold to nearly 1000-fold increase in intracellular concentrations have been reported),[9] highlighting the variability in regulating/disregulating metabolic pathways in different cells. These observations suggest that selectivity in biochemical interventions may be possible, even when targeting a critical step in an important metabolic pathway.

Currently, nitrogen-containing bisphosphonate drugs (*N*-BPs) are the only clinically relevant compounds that inhibit hFPPS.[10,11] Bisphosphonates are chemically stable bioisosteres of pyrophosphates and structurally characterized by two phosphonate groups attached to a central carbon (Cα) instead of an oxygen atom. Additionally, one of the Cα substituents (i.e., the *N*-BP side chain) is usually characterized by a basic nitrogen atom, presumed to be protonated under physiological conditions and mimicking the interactions of the putative allylic carbocation transition state that forms during the hFPPS catalytic cycle.[12] The structure of the most potent *N*-BP drugs, such as zoledronic acid (**1**) and risedronic acid (**2a**), is also characterized by a Cα-hydroxyl moiety, which maximizes their affinity for the bone mineral hydroxyapatite (HAP).[13,62] The Cα-hydroxyl moiety also participates in additional interaction with the active site of the enzyme, thus contributing to the potency of these compounds.[10,13]

N-BP drugs are routinely used to treat osteoporosis and other lytic bone diseases, including bone cancer metastasis and multiple myeloma (MM).[14−16] *N*-BPs bind so strongly to bone that their half-life (in bone) can be months to several years, depending on the type of drug and the degree of bone turnover.[17,18] In chronic diseases (e.g., osteoporosis), concerns that prolonged use of *N*-BPs can lead to side effects, such as osteonecrosis of the jaw and atypical femoral fractures, have led to the recommendation by physicians of a "drug holiday". However, this treatment can lead to uncertainty with respect to the type of drug that should be used and the duration of treatment for different patients.[19] Furthermore, the systemic half-life of current *N*-BPs is extremely low; for example, after iv administration of **1**, 50% of the dose gets trapped in the bone mineral and the rest is rapidly cleared by the kidneys (the dose-limiting toxicity of **1** is based on nephrotoxicity).[20,21]

In spite of their poor drug-like properties (including extremely low cell membrane permeability and oral bioavailability), recent clinical investigations provide evidence that some *N*-BP drugs (e.g., **1**) are disease modifying agents that improve the survival of patients with multiple myeloma (MM) via mechanisms that are both related as well as unrelated to the skeletal benefits.[22,23] Similar results were reported for patients with premenopausal breast cancer,[24] although these findings seem to be more controversial.[25] Nonetheless, the identification of hFPPS inhibitors with superior oral bioavailability, half-life in plasma (i.e., slower rates of elimination from the blood circulation), and higher nonskeletal tissue distribution may provide effective antiresorptive agents that are also more effective in cancer chemotherapy than the current *N*-BP drugs. In this report, we describe our structure−activity relationship (SAR) studies on thienopyrimidine-based bisphosphonate (ThP-BP) inhibitors of hFPPS and the identification of analogues with low nanomolar potency. Co-crystal structures of two ThP-BP analogues bound to the allylic subpocket of hFPPS (i.e., the DMAPP/GPP binding subpocket of the active site) revealed details of the protein−inhibitor interactions and conformational changes to the C-terminal region that lead to closing of the active site cavity. These ThP-BP molecules are significantly less hydrophilic than the current *N*-BP drugs but exhibit high affinity for the bone mineral hydroxyapatite. The in vitro affinity of bisphosphonates for hydroxyapatite is known to correlate well with the in vivo affinity of the *N*-BP drugs for bone.[13,62] Thus, the ThP-BP compounds are promising new leads for medicinal chemistry studies that aim to identify new inhibitors of hFPPS with better biopharmaceutical properties than those of the current *N*-BP drugs.

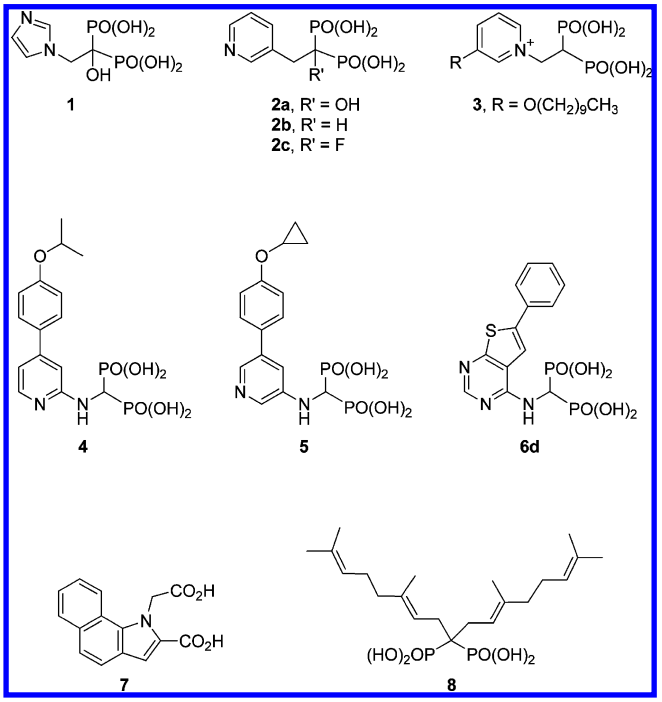

CHEMISTRY

In our search of new structural classes of hFPPS inhibitors, we recently identified thienopyrimidine-based bisphosphonates (ThP-BPs; e.g., **6d**) with modest in vitro potency in inhibiting hFPPS.[26] The thienopyrimidine scaffold is considered to be

dx.doi.org/10.1021/jm400946f | J. Med. Chem. 2013, 56, 7939−7950

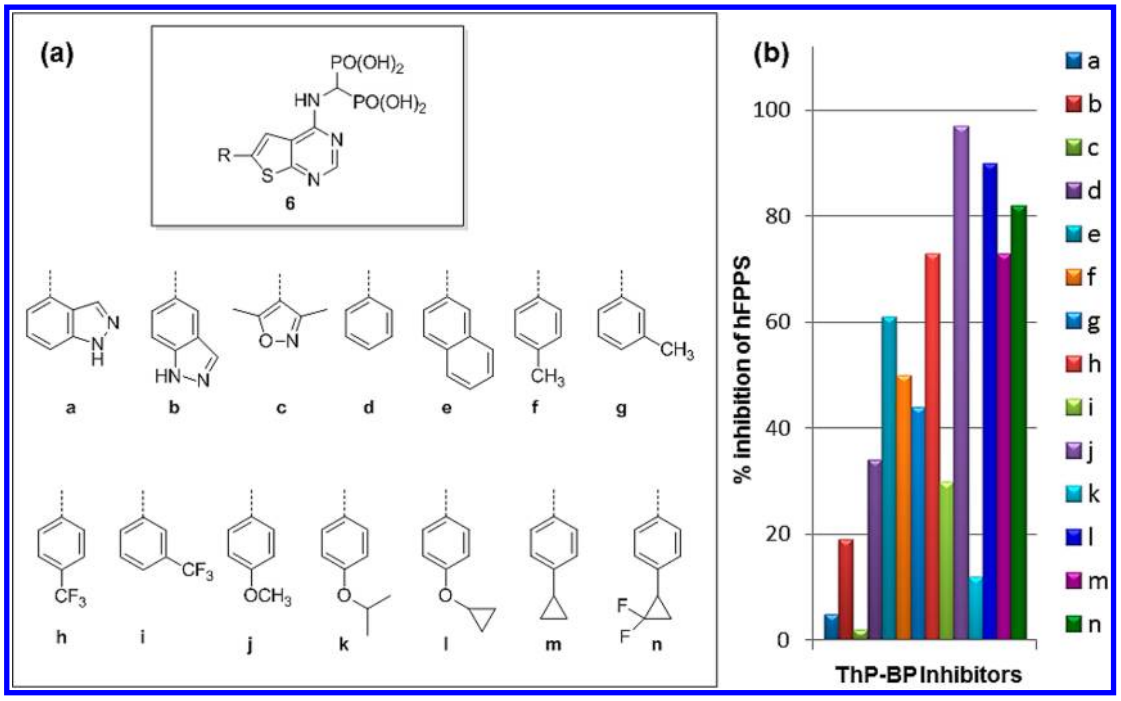

Figure 1. Thienopyrimidine inhibitors of the human FPPS. (a) Representative examples of analogues. (b) Inhibition of hFPPS at 100 nM concentration of each compound using the M2 assay (average of three determinations; standard deviation ≤10%).

privileged in drug discovery due to its inherently favorable biopharmaceutical profile. Thienopyrimidine-based compounds are currently under investigation as therapeutics for the treatment of many diseases, including fungal[27] and viral infections[28] and cancer.[28−36]

At the time of our initial report on ThP-BPs,[26] the mechanism by which these compounds inhibit hFPPS was unclear. Given the significantly larger molecular size of ThP-BPs (e.g., **6d**) as compared to the current *N*-BP drugs (e.g., **1** and **2a**), we presumed that their binding interactions with hFPPS may also be different. Mindful of the conformational plasticity of this enzyme that permit the binding of fairly large *N*-BP molecules (e.g., **4**) in the allylic subpocket, we prepared a focused library of ThP-BP derivatives guided by our previous SAR studies (e.g., SAR derived from pyridine analogues such as **4** and **5**);[37,38] some representative examples are shown in Figure 1.

The synthesis of the ThP-BP analogues was initiated from the key fragment 6-bromothieno[2,3-*d*]pyrimidin-4-amine (**10**), which was prepared via the trimethylsilyl ylidine **9** as previously described (Scheme 1).[26] Intermediate **10** was also prepared starting from 2,5-dihydroxy-1,4-dithiane (**12**), via the unsubstituted 2-amino-thiophene-3-carbonitrile core, following earlier literature procedures.[39,40] Although the two synthetic protocols (paths A and B) are equivalent in the overall number of steps leading to **10**, the average isolated yield via pathway A was significantly higher (Scheme 1; the average overall yield of **10** was 18% vs 8% obtained via pathways A and B, respectively).

Conversion of **10** to the bisphosphonate tetraester **11** was easily achieved upon treatment with triethoxymethane and diethylphosphite. Cross coupling of **11** with a variety of boronate esters, under typical Suzuki conditions, followed by hydrolysis of the tetraethyl bisphosphonate esters **13** with TMSBr/MeOH, resulted in the formation of the final thienopyrimidine bisphosphonic acids of general structure **6** (Scheme 1).

Scheme 1. Synthesis of C-6 Substituted Thieno[2,3-*d*]pyrimidin-4-amine-Based Bisphosphonate Inhibitors of hFPPS[a]

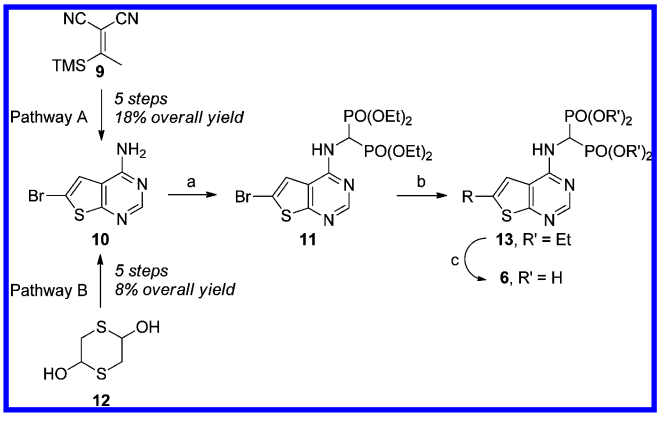

[a]Conditions: (a) $CH(OEt)_3$, diethylphosphite, 130 °C, 24 h (75%); (b) 10 mol % $Pd(PPh_3)_4$, KF, MeOH, 120 °C, μW, 20 min; (c) TMSBr, MeOH, RT, 72 h (overall isolated yield for steps (b) and (c) ranged from ∼20% to 80%).

RESULTS AND DISCUSSION

Metabolic disregulation of hFPPS has been implicated in many human diseases, including various cancers (e.g., breast, prostate, and MM) and neurodegenerative diseases such as the Alzheimer's disease.[41,42] However, in vivo investigation of hFPPS as a therapeutic target is hampered by the lack of molecular tools that can selectively inhibit this enzyme and can exhibit significant in vivo distribution into soft tissues. Past efforts toward improving the clinical use of *N*-BPs have included investigations of pro-drugs,[43,44] improved drug

dx.doi.org/10.1021/jm400946f | J. Med. Chem. 2013, 56, 7939−7950

formulations,[45] and structural modifications that may increase oral bioavailability and decrease the rate of compound clearance from circulation. *N*-BPs with more lipophilic side chains (e.g., **3**,[46,47] **4**, **5**) than the clinical drugs **1** and **2a**, as well as bicyclic heterocyclic side chains, have been explored, including imidazopyridines, benzimidazoles,[48] and azaindoles.[49,50] To the best of our knowledge, none of these efforts have produced an hFPPS inhibitor with superior clinical profile than that of analogues **1** or **2a**. We recently identified thienopyrimidine-based bisphosphonates (ThP-BPs) with IC_{50} potency in inhibiting hFPPS in the 0.5−1 μM range. These hits were used for further SAR studies and optimized into low nanomolar inhibitors of hFPPS.

It is noteworthy that several different assays have been reported in the literature for evaluating in vitro hFPPS inhibition. The most commonly used method was originally developed by Reed and Rilling[51] and has been adopted by many researchers with only minor modifications;[13,37,38,53] we refer to these conditions as method 1 (M1). The IC_{50} values of hFPPS inhibitors can vary considerably, depending on the assay method; for example, the reported IC_{50} values of **1** range from approximately 4 nM[11,52,53] to 200 nM,[54] and can be as high as 475 nM if the compound is tested without preincubation with the enzyme.[53] Experimental artifacts in a functional assay can further contribute to the observed potency of a compound and mislead SAR studies. Lipophilicity-dependent aggregation of moderately (or poorly) hydrophilic compounds is the most common factor responsible for false experimental data and can affect both in vitro and cell-based assays.[55] The ability of bisphosphonates to form stable, high-order complexes in solution, particularly in the presence of metal ions, is a well-documented phenomenon, exploited in a number of biomedical applications.[56−58] The high charge density of the magnesium cation may also play a role in augmenting the solvent-induced interaction between the hydrophobic side chains of the ThP-BP inhibitors (as compared to smaller and more polar *N*-BPs; CLogP values are shown in Table 1).[72] A combination of these effects appear to induce significant aggregation under the M1 assay conditions and lead to artifacts in characterizing hFPPS inhibition. A number of assay modifications were investigated, including lowering the concentration of Mg^{2+} ions and adding Triton X-100 (0.01%) in the assay buffer. The addition of Triton X-100 in the buffer was previously reported for testing nonbisphosphonate inhibitors of hFPPS.[59,60] The ratio of hFPPS protein, IPP/GPP substrates, and Mg^{2+} ion concentrations were also optimized in order to achieve maximum catalytic turnover and highest sensitivity in detecting weakly active compounds; we refer to these conditions as assay method 2 (M2).

Table 1. Inhibition Data for Key Compounds

	hFPPS IC_{50} (nM)[a]		
compd	M1 assay	M2 assay	CLogP of side chain moiety
1	*4.1*[b]	nd[c]	−0.84
2a	11	5.2	−0.16
5	16	18	3.6
7	∼20000	920	nd
6e	250	63	5.0
6f	390	22	4.3
6j	440	15	3.7
6h	nd	21	4.7
6k	nd	200	4.6
6l	nd	14	4.3
6m	115	39	4.8
6n	140	11	4.1

[a]Average IC_{50} values of a minimum of three determinations (standard deviation ≤10). All compounds were also tested in our hGGPPS inhibition assay, and none were active at concentration up to 10 μM. [b]IC_{50} value reported by Kavanagh et al.[53] CLogP values were estimated without the two phosphonate groups in order to simplify the calculations. [c]Value was not determined (nd).

The IC_{50} values of several known hFPPS inhibitors were determined using both the M1 and M2 assay conditions. Little variability (≤2-fold) was observed in the observed potency of pyridine-based *N*-BP molecules (Table 1; analogue **2a** and **5**). In contrast, the IC_{50} of the hFPPS allosteric inhibitor **7** was approximately 22-fold lower in the M2 assay than the M1 assay and ∼100-fold lower than the value reported using yet another assay protocol;[61] the IC_{50} values of **7** were determined to be ∼20 and 0.92 μM in the M1 and M2 assay, respectively (Table 1). The IC_{50} values for our initial hits, **6e** and **6f**, were also lower in the M2 assay as compared to the M1 assay (Figure 1a, Table 1). A defining characteristic of molecular aggregation is the formation of higher-order soluble particles on the submicrometer scale that are disrupted (to some degree) by the presence of a detergent such as Triton X-100, Tween-20, or Tween-80.[55] The higher propensity of ThP-BPs to aggregate in the assay buffer, as compared to the *N*-BP analogue **2a**, was confirmed by dynamic light scattering (DLS); aggregation was particularly pronounced in the presence of high Mg^{2+} concentrations (an example is shown in Supporting Information Figure 1).

The optimized M2 assay was subsequently adopted for our routine biological screening of all ThP-BP inhibitors. All analogues were initially tested at a concentration of 1.0 and 0.1 μM; representative examples are shown in Figure 1. The general potency profile for these compounds was similar to the SAR previously observed with 2-amino- and 3-aminopyridine libraries.[37,38] For example, analogues with polar heterocyclic side chains, such as **6a**, **6b**, and **6c**, exhibited weak activity in inhibiting hFPPS (<20% inhibition was observed at 100 nM), and *meta*-substituted phenyls were less potent than their corresponding *para*-analogues (e.g., analogues **3h** and **3i** exhibited 73% vs 30% inhibition at 100 nM, respectively). Full dose−response inhibition curves were obtained only for analogues deemed critical to our SAR studies and analogues exhibiting >50% inhibition at 100 nM. A number of novel thienopyrimidine-based inhibitors of hFPPS were identified with IC_{50} values in the 10−50 nM range; representative examples are shown in Table 1. In addition, all analogues with an IC_{50} <100 nM were tested in our in vitro hGGPPS inhibition assay, using compound **8** as the positive control, as previously reported;[37] none of these compounds were active at concentration up to 10 μM; the buffer of our hGGPPS inhibition assay contained 0.2% Tween-20 (i.e., 20-fold higher concentration of detergent than our M2 hFPPS inhibition assay), which should minimize or eliminate any effects due to aggregation.

It has been shown that *N*-BPs such as **1**, that bind very strongly to bone and get rapidly eliminated from plasma, achieve extremely low concentrations in most noncalcified tissues.[21] Consequently, their therapeutic efficacy as antitumor agents for *non*-bone-related cancers is greatly compromised. The Cα-hydroxy bisphosphonate moiety of the current drugs

(**1** and **2a**) is generally believed to enhance bone affinity by allowing a tridentate interaction with Ca^{2+} ions and the bone mineral hydroxyapatite. Consistent with this assumption, replacement of the Cα-hydroxy group with a proton (e.g., **2b**) or a halogen (e.g., **2c**) was shown to decrease both the affinity for the bone mineral hydroxyapatite and the ability of the compounds to inhibit hFPPS.[13] The in vitro affinity of bisphosphonates for hydroxyapatite is known to correlate well with the in vivo affinity of the *N*-BP drugs for bone.[13,62] We compared the relative binding affinity of ThP-BPs **6m** and *N*-BP **2a** for hydroxyapatite (HAP) using the NMR protocol reported by Jahnke and Henry.[62] After incubation with HAP, changes in the relative intensity of the aromatic proton signals were observed for both compounds. However, a much more significant decrease in the intensity of the aromatic signals of analogue **6m** was observed as compared to **2a**, consistent with a higher portion of **6m** binding to HAP and removed from the solution (Figure 2). Similar results were also obtained with

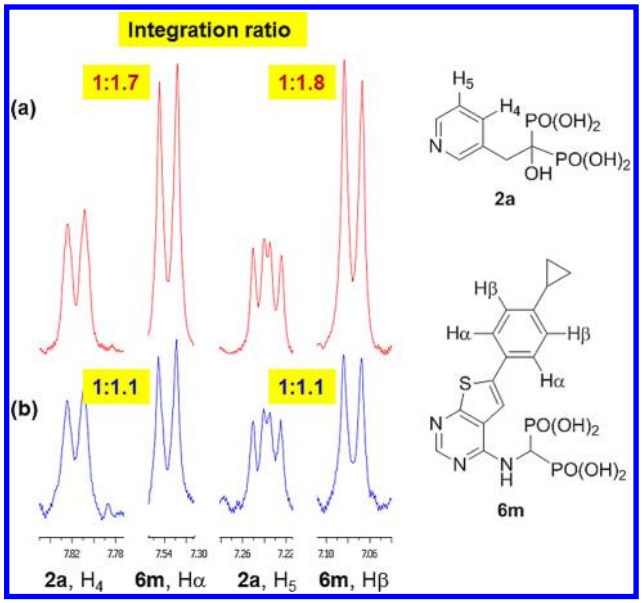

Figure 2. Differentiation of **2a** and **6m** in their competitive binding to HAP (for clarity, only select regions of the ^{1}H NMR spectra are shown). (a) ^{1}H NMR spectra of **2a** and **6m** at approximately 1:1 molar ratio (~50 μM of each compound) in Tris buffer before any treatment. (b) ^{1}H NMR spectrum of the same solution of **2a** and **6m** as that used to acquire the spectrum shown in (a) after incubation with 0.8 mg of HAP at room temperature for 5 min.

analogues **6h** and **6l**, suggesting that this high affinity for hydroxyapatite is likely structure-dependent. These results are somewhat surprising because it is generally believed that the Cα-hydroxyl substituent of *N*-BPs provides the optimal "bone hook" and contributes to the antiresorptive efficacy of the current *N*-BP drugs. Differences in lipophilicity and bone affinity can potentially affect the pharmacokinetic and pharmacodynamics properties of these compounds, thus contributing to a unique therapeutic profile.

Clinical evidence is rapidly accumulating which implicates inhibitors of hFPPS as antineoplastic and specifically antimyeloma therapeutic agents.[22,23] Antiproliferation and cytotoxic effects were observed with inhibitor **6m** that compared favorably to the effects of **1** and **2a** (Table 1). Treatment of human MM cell line RPMI-8226 with each of the three compounds resulted in reductions of cell proliferation with median effective concentrations for 50% growth inhibition (EC_{50}) of 11, 13, and 8.5 μM, for **1**, **2a**, and **6m**, respectively (Table 2); values represent the average of $n \geq 8$ determinations with R^2 in the range of 0.90−0.98.

Table 2. Antiproliferation Effects in the Multiple Myeloma Cells

compd	hFPPS IC_{50} (nM) M2 assay	EC_{50} (μM)[a] cell line RPMI-8226
1	nd[b]	11
2a	5.2	13
6m	39	8.5

[a]Average EC_{50} values of $n \geq 8$ determinations; R^2 values in the range of 0.90-0.98. [b]Value was not determined (nd).

Finally, two representative ThP-BP inhibitors, **6f** and **6m**, were also cocrystallized with hFPPS (Table 2). Both compounds were found to bind in the allylic subpocket of the active site in the same manner without causing major conformational strain to the protein despite their bulky and rigid side chains. However, unlike **1** and **2a** (which bind to only a small portion of the allylic subpocket), the interactions of **6f** and **6m** with the active site cavity extend through the capping phenyls (Phe 98/99) and toward the hFPPS dimer interface. Some of the key features of these binding interactions are illustrated with the hFPPS−**6m**−PPi ternary complex (PDB 4L2X) in Figure 3. The simulated annealing omit map clearly demonstrates the presence of bound **6m**, as well as three magnesium ions and water molecules, which mediate the interaction between the bisphosphonate moiety and the two DDXXD motifs of the protein (Figure 3a). Some of the metal-mediated interactions between the bisphosphonate and aspartic acid residues of the DDXXD motifs are direct, whereas others are water mediated. There are three additional interactions between the positively charged residues Arg 112, Lys 200, and Lys 257, which make direct contacts with the bisphosphonate moiety of the inhibitor, which are not shown in Figure 3a for clarity. The side chain of **6m** fills the lipophilic cavity of the allylic subpocket completely, with its cyclopropyl tail extending to the end of the cavity at the dimerization interface (Figure 3b). The phenyl ring of the **6m** side chain is engaged in stacking interactions with the side chains of Phe 99 and Gln 171, similarly to what was previously observed with inhibitor **4** (Figure 3c).[37,63]

The thienopyrimidine scaffold also displaces the side chain hydroxyl of Thr 201 and the main chain carbonyl of Lys 200 by ~0.65 Å; these residues are presumed to participate in a bifurcated H-bond interaction with the protonated side chain of **1** (Figure 3c). The hFPPS−**6m**−PPi complex adopts a fully closed conformation, similar to that observed in the hFPPS−**1**−IPP ternary complex (PDB 1ZW5).[10] Superposition of our hFPPS−**6m**−PPi structure with the structure of the hFPPS−**1**−IPP ternary complex (Figure 3d) revealed the same folding of the ^{350}KRRK^{353} C-terminal tail over the IPP subpocket. These data are consistent with our earlier observations indicating that following occupancy of the allylic subpocket, inorganic pyrophosphate (PPi) can play the same role as IPP in inducing the closing of the hFPPS active site cavity.[63] Previous investigations suggested that this secondary ligand-induced conformational change of the C-terminal basic residues (^{350}KRRK^{353}) leads to a nearly irreversible inhibition of the

dx.doi.org/10.1021/jm400946f | J. Med. Chem. 2013, 56, 7939−7950

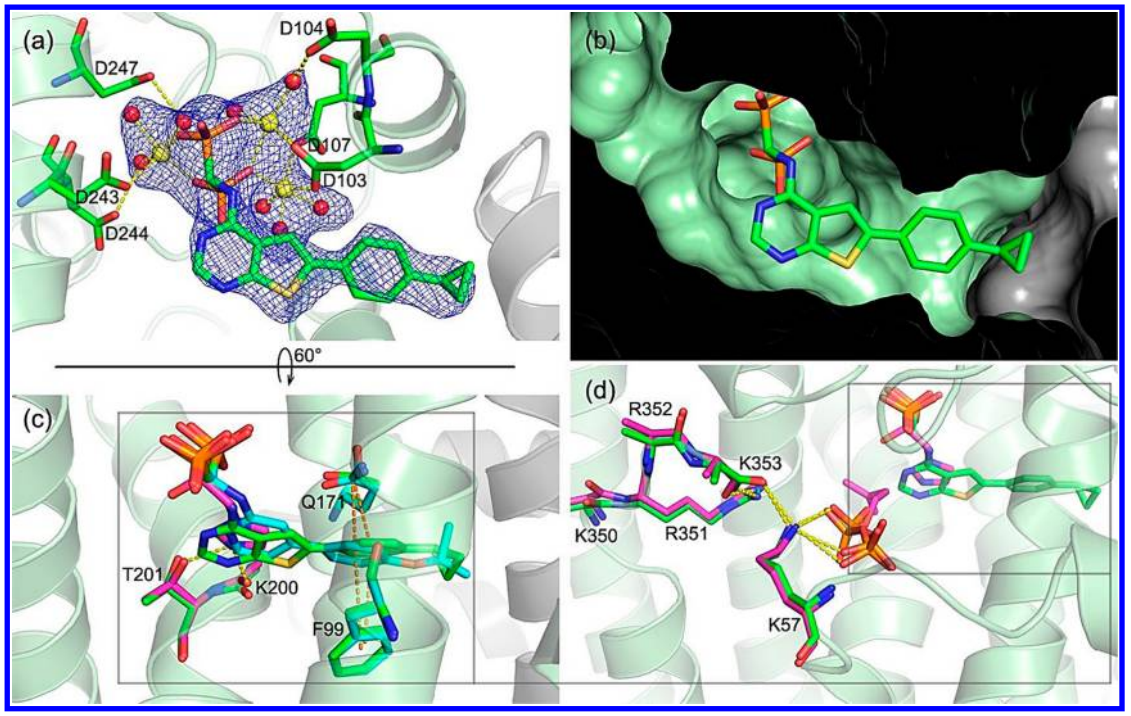

Figure 3. Crystal structure of hFPPS in complex with analogue **6m** (PDB 4L2X); key interactions are indicated with dashed yellow lines. (a) The blue mesh represents a simulated annealing omit map ($F_o - F_c$, contoured at 3σ) for the bisphosphonate ligand, magnesium ions (yellow spheres), and coordinated water molecules (red spheres). In addition to the Mg^{2+}-mediated bisphosphonate interactions with the aspartic acid residues (some direct and others via water molecules), there are three direct interactions between the bisphosphonate and Arg 112, Lys 200, and Lys 257, which are not shown for clarity. (b) A cross section view of the allylic (GPP) subpocket rendered in a surface representation. The allylic pocket is blocked at one end by the adjacent monomer (hFPPS exists as a homodimer with an active site in each monomer), which is shown in gray. (c) Superimposition of the *N*-BP inhibitors **1**, **4**, and the ThPBP analogue **6m** in three cocrystal structures. Carbon atoms are represented in green, cyan, and magenta for the hFPPS−**1**−IPP (PDB 1ZW5), hFPPS−**4**−PPi (PDB 4H5D), and hFPPS−**6m**−PPi (PDB 4L2X) ternary complexes, respectively. The color representation for heteroatoms is: blue for nitrogen, red for oxygen, orange for phosphorus, and yellow for sulfur. The secondary ligands (i.e., PPi or IPP) are omitted for clarity. (d) Closing of the active site in the presence of bound IPP or PPi. The ^{350}KRRK^{353} tail and Lys 57 are rigidified in both the hFPPS−**1**−IPP and hFPPS−**6m**−PPi complexes. The side chains of Arg 352 and Lys 353 are not shown for clarity. The potential steric clash between the thienopyrimidine core of **6m** and the prenyl side chain of IPP is evident (closest carbon-to-carbon contact is less than 2.7 Å).

enzyme and is partly responsible for the excellent in vivo efficacy of the bisphosphonate compounds.[64]

In addition, our crystal structure suggested that cobinding of IPP and inhibitor **6m** was unlikely due to a potential steric clash between the thienopyrimidine core of **6m** and the prenyl side chain of IPP (Figure 3d). This prediction was confirmed by determining the thermal stability of the hFPPS complexes using differential scanning fluorimetry (DSF).[65] A substantial difference in thermal stability was observed for the hFPPS−**2a** and hFPPS−**4** complexes in the presence or absence of IPP ($\Delta\Delta T_m$) of approximately +8 °C and +14 °C, respectively (Figure 4a,b). The thermal stability difference observed between the hFPPS−**2a** and hFPPS−**2a**−IPP complexes is consistent with a $\Delta\Delta T_m$ of +8.3 °C, measured using differential scanning calorimetry (DSC) under the same ratio of ligands (i.e., **2a**:IPP in 1:1 ratio).[10] In contrast, parallel titration of hFPPS with **6m** and IPP showed no significant difference in the thermal stability of these complexes (Figure 4c; $\Delta\Delta T_m \leq 1$ °C), suggesting that cobinding of **6m** and IPP was prohibited.

■ CONCLUSIONS

Herein we disclose the hit-to-lead optimization of a new series of thienopyrimidine-based bisphosphonate (ThP-BP) inhibitors of hFPPS, which led to the identification of compounds with low nanomolar potency. The crystal structures of the hFPPS−**6f**−SO_4 and hFPPS−**6m**−PPi ternary complexes revealed that the inhibitors bind to the allylic subpocket of the active site and their side chain extends through the capping phenyls and toward the protein dimer interface. The side chain of these inhibitors engages in stacking interactions with both Phe 99 and Gln 171, as we previously observed with inhibitor **4**.[37,63] A number of other conformational changes within the active site were also observed, including the closing of the C-terminal tail over the IPP subpocket, which was induced by inorganic pyrophosphate (PPi). Our X-ray structures and the DSF thermal stability data of the hFPPS−**6m** complex also suggest that the ThP-BP inhibitors compete for binding with both natural substrates of hFPPS (i.e., DMAPP/GPP and IPP) and occupy (*in part*) both subpockets of the active site cavity. Significant physicochemical differences between the ThP-BP compounds and the current *N*-BP drugs include higher lipophilicity and higher affinity for the bone mineral hydroxyapatite. Analogue **6m**, which exhibits good in vitro potency and a high lipophilicity, was also shown to inhibit proliferation of human multiple myeloma cells (RPMI 8226) with equivalent potency to *N*-BPs **1** and **2a**. Thus further lead optimization of the ThP-BP analogues is warranted and currently in progress. The higher lipophilicity of these compounds could result in lower rate of elimination from plasma, higher volume of distribution into nonskeletal tissue, and better therapeutic value for treating multiple myeloma and other nonskeletal cancers.

dx.doi.org/10.1021/jm400946f | *J. Med. Chem.* 2013, 56, 7939−7950

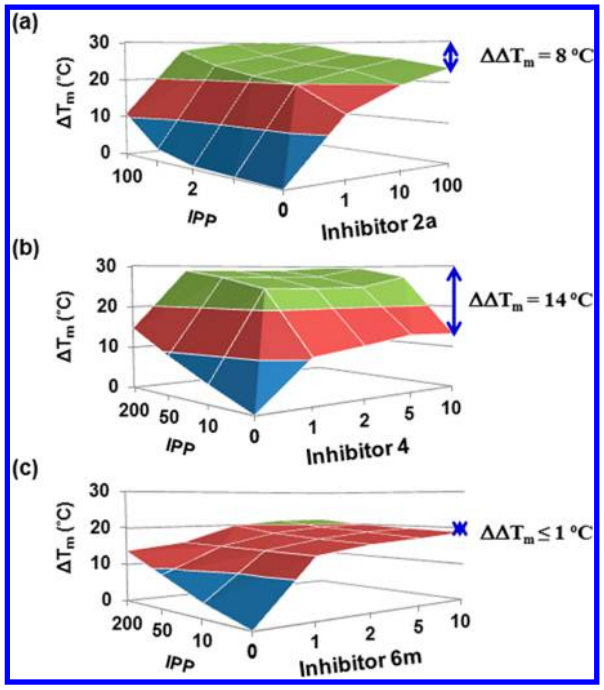

Figure 4. Differential scanning fluorimetry (DSF) surface plots showing concentration-dependent increase in thermal stability of hFPPS–inhibitor–IPP complexes; hFPPS concentration fixed at 4 μM; the x/y axis indicates IPP:inhibitor molar ratios relative to the concentration of hFPPS. (a) Co-binding of inhibitor **2a** and IPP to hFPPS. (b) Co-binding of inhibitor **4** and IPP to hFPPS. (c) Co-titration of inhibitor **6m** and IPP to a solution of hFPPS; plot suggests the simultaneous binding of **6m** and IPP in the hFPPS active site does not occur.

EXPERIMENTAL SECTION

General Procedures for Characterization of Compounds. All analogues **13** were purified by normal phase flash column chromatography using a CombiFlash instrument on silica gel and a solvent gradient from 5% EtOAc in hexanes to 100% EtOAc and then to 20% MeOH in EtOAc unless otherwise indicated. The homogeneity of all analogues **13** was confirmed by reverse-phase HPLC. Only bisphosphonate esters **13** with homogeneity ≥95% were processed further though the hydrolysis step to the final bisphosphonic acid inhibitors **6a–n**. IC_{50} values were determined only for final compounds **6a–n** with ≥95% homogeneity. HPLC Analysis was performed using a Waters ALLIANCE instrument (e2695 with 2489 UV detector and 3100 mass spectrometer). Each analogue of **13** and **6** was fully characterized by ^{1}H, ^{13}C, and ^{31}P NMR and MS. Chemical shifts (δ) are reported in ppm relative to the internal deuterated solvent (^{1}H, ^{13}C) or external H_3PO_4 (δ 0.00 ^{31}P) unless indicated otherwise. The high-resolution MS spectra of final products **6a–n** were recorded using electrospray ionization ($ESI^{\pm}$) and Fourier transform ion cyclotron resonance mass analyzer (FTMS).

Method. (homogeneity analysis using a Waters Atlantis T3 C18 5 μm column): Solvent A: H_2O, 0.1% formic acid. Solvent B: CH_3CN, 0.1% formic acid. Mobile phase: linear gradient from 95%A and 5%B to 5%A and 95%B in 13 min, then 2 min at 100% B. Flow rate: 1 mL/min.

Synthesis of Tetraethyl (((6-Bromothieno[2,3-d]pyrimidin-4-yl)-amino)methylene)bis(phosphonate) (11). A solution of 6-bromothieno[2,3-*d*]pyrimidin-4-amine (**10**, 500 mg, 2.173 mmol, 1 equiv) in anhydrous toluene (20 mL) was flushed with argon in a pressure vessel. Diethylphosphite (1.96 mL, 15.2 mmol, 7 equiv) and triethyl orthoformate (0.61 mL, 3.69 mmol, 1.7 equiv) were added to the reaction mixture via syringe, and the reaction mixture was argon flushed, sealed, and stirred at 130 °C in the dark for 48 h. The crude mixture was concentrated to dryness under vacuum. The crude product was purified by normal phase flash column chromatography on silica gel using a CombiFlash instrument and a solvent gradient from 20% EtOAc/hexanes to 100% EtOAc and 100% EtOAc to 20% methanol/EtOAc to give intermediate **11** as a pale-yellow solid (834.2 mg, 74% isolated yield). ^{1}H NMR (400 MHz, CD_3OD): δ 8.44 (s, 1H), 7.85(s, 1H), 5.96 (t, J = 23.7 Hz, 1H), 4.24–4.17 (m, 8H), 1.31–1.25 (m, 12H). ^{13}C NMR (75 MHz, CD_3OD): δ 168.7, 156.2, 154.5, 123.1, 119.1, 113.4, 65.2–65.0 (m), 45.6 (t, J = 150.2 Hz), 16.7–16.6 (m). ^{31}P NMR (81 MHz, D_2O): δ 17.2. MS (ESI–) m/z $[M + H]^+$: 514.1.

General Protocol for the Suzuki Cross-Coupling Reactions Using Fragment 11. Suzuki coupling reactions were run in parallel using aliquots of fragment **11** (~40 mg) and various boronate esters (1.4 equiv); examples are shown in Figure 1. All reactions were carried out in MeOH (purged with argon, both before and after the addition of reagents), in an argon flushed microwave reactor vial, at 120 °C for 20 min (120W), catalyzed by $Pd(PPh_3)_4$ (0.1 equiv) and KF (2.5 equiv). The crude mixtures were filtered through Celite, concentrated to dryness under vacuum, and purified using automation as described in the general procedures.

General Protocol for the Hydrolysis of the Esters 13 to Give the Final Inhibitors 6a–n. A solution of the tetraethyl bisphosphonate ester (1 equiv) in CH_2Cl_2 was cooled to 0 °C, and trimethylsilyl bromide (15 equiv) was added via syringe. The reaction mixture was stirred at room temperature for 3–5 days; completion of conversion was monitored by ^{31}P NMR. The mixture was then concentrated under vacuum, diluted with HPLC grade MeOH (~5 mL), and the solvent was evaporated to dryness; this step was repeated four times. The organic solvents were evaporated under vacuum, the residue was suspended in 0.5 mL MeOH, and H_2O (~5 mL Milli-Q grade) was added to induce precipitation of the thienopyrimidine bisphosphonic acid **6**. The amorphous powder was collected by filtration, washed with deionized water (2×), HPLC-grade CH_3CN (2×), and with distilled Et_2O or toluene (2×). The residue was then dried under vacuum to give the final compound **6a–n** as a solid; it should be noted that although the conversion of **13** to **6** was quantitative (as determined by HPLC and ^{13}P NMR), the isolated yields varied depending on the solubility of each final products.

(((6-(1H-Indazol-4-yl)thieno[2,3-d]pyrimidin-4-yl)amino)-methylene)diphosphonic Acid (6a). Isolated as a yellow solid, 18.5

Table 3. Data Collection and Refinement Statistics[a]

Data Sets		
PDB ID	4JVJ	4L2X
ligands	inhibitor **6f**, SO_4	inhibitor **6m**, PPi
Data Collection		
space group	$P4_12_12$	$P4_12_12$
unit cell dimension (Å)	$a = b = 111.33$, $c = 67.46$	$a = b = 111.34$, $c = 68.77$
resolution range (Å)	50.0–2.80 (2.85–2.80)	50.0–2.55 (2.62–2.55)
redundancy	9.5 (9.6)	9.5 (9.5)
completeness (%)	98.6 (99.6)	98.3 (93.8)
$I/\sigma(I)$	27.3 (6.6)	24.0 (6.1)
R_{merge}	0.073 (0.260)	0.052 (0.382)
Refinement		
no. reflections	10170	13394
no. protein atoms	2648	2687
no. ligand atoms	31	37
no. ion atoms	3	3
no. solvent atoms	14	15
R_{work}/R_{free}	0.236/0.288	0.201/0.257
rms Deviations		
bond length (Å)	0.011	0.013
bond angle (deg)	1.4	1.7

[a]Values in parentheses are for the highest resolution shell.

dx.doi.org/10.1021/jm400946f | J. Med. Chem. 2013, 56, 7939–7950

mg (66% overall isolated yield). ^{1}H NMR (500 MHz, D_2O): δ 8.30 (overlapping singlets, 2H), 7.31−7.29 (m, 2H), 7.15−7.12 (m, 2H); central methylene proton obscured by solvent signal (confirmed by HSQC). ^{13}C NMR (126 MHz, D_2O): δ 162.8, 156.0, 153.3, 140.6, 137.1, 132.5, 126.7, 125.7, 119.7, 118.7, 118.0, 115.6, 110.9, 50.4 (t, J = 124.9 Hz). HSQC (^{1}H−^{13}C): ^{1}H δ 4.57 correlates with ^{13}Cα δ 50.4. ^{31}P NMR (81 MHz, D_2O): δ 13.8. HRMS (ESI−) calculated for $C_{14}H_{12}N_5P_2O_6S$ m/z [M − H]$^-$, 439.99890; found, m/z 439.99914.

*(((6-(1H-Indazol-5-yl)thieno[2,3-d]pyrimidin-4-yl)amino)-methylene)diphosphonic Acid (**6b**).* Isolated as a pale-pink solid, 14.9 mg (17% overall isolated yield). ^{1}H NMR (500 MHz, D_2O): δ 8.02 (s, 1H), 7.65 (d, J = 8.2 Hz, 1H), 7.59 (s, 1H), 7.55 (s, 1H), 7.50 (d, J = 8.2 Hz, 1H), 6.94 (s, 1H) ; central methylene proton obscured by solvent signal. ^{13}C NMR (126 MHz, D_2O): δ 161.7, 155.4, 152.8, 139.2, 139.1, 133.3, 125.8, 124.3, 122.1, 118.1, 117.9, 112.9, 111.8, Cα observed by HSQC. HSQC (^{1}H−^{13}C): ^{1}H δ 4.56 correlates with ^{13}C δ 50.8. ^{31}P NMR (81 MHz, D_2O): δ 13.9. HRMS (ESI−) calculated for $C_{14}H_{12}N_5P_2O_6S$ m/z [M − H]$^-$, 439.99890; found, m/z 439.99912.

*(((6-(3,5-Dimethylisoxazol-4-yl)thieno[2,3-d]pyrimidin-4-yl)-amino)methylene)diphosphonic Acid (**6c**).* Isolated as a white solid, 18.2 mg (39% overall isolated yield). ^{1}H NMR (500 MHz, D_2O): δ 8.29 (s, 1H), 7.56 (s, 1H), 4.63 (t, J = 18.9 Hz, 1H), 2.56 (s, 3H), 2.40 (s, 3H). ^{13}C NMR (126 MHz, D_2O): δ 167.9, 163.5, 159.8, 156.1, 153.5, 126.6, 118.5, 117.7, 110.1, 50.8 (t, J = 125.9 Hz), 11.4, 10.2. ^{31}P NMR (81 MHz, D_2O): δ 13.6. HRMS (ESI−) calculated for $C_{12}H_{13}N_4P_2O_7S$ m/z [M − H]$^-$, 418.9986; found, m/z 418.9985.

*(((6-(m-Tolyl)thieno[2,3-d]pyrimidin-4-yl)amino)methylene)-diphosphonic Acid (**6g**).* Isolated as a pale-yellow solid, 25.5 mg (55% overall isolated yield). ^{1}H NMR (500 MHz, D_2O): δ 8.28 (s, 1H), 7.87 (s, 1H), 7.65 (s, 1H), 7.60 (d, J = 7.8 Hz, 1H), 7.40 (t, J = 7.8 Hz, 1H), 7.27 (d, J = 7.8 Hz, 1H), 4.63 (t, J = 18.8 Hz, 1H), 2.39 (s, 3H). ^{13}C NMR (126 MHz, D_2O): δ 163.2, 156.2, 153.5, 139.5, 139.4, 133.1, 129.3, 129.2, 126.5, 123.0, 118.6, 114.6, 20.3, Cα observed by HSQC. HSQC (^{1}H−^{13}C): ^{1}H δ 4.63 correlates with ^{13}C δ 51.0. ^{31}P NMR (81 MHz, D_2O): δ 13.7. HRMS (ESI−) calculated for $C_{14}H_{14}N_3P_2O_6S$ m/z [M − H]$^-$, 414.00840; found, m/z 414.00848.

*(((6-(4-(Trifluoromethyl)phenyl)thieno[2,3-d]pyrimidin-4-yl)-amino)methylene)diphosphonic Acid (**6h**).* Isolated as a yellow solid, 25.4 mg (52% overall isolated yield). ^{1}H NMR (500 MHz, D_2O): δ 8.29 (s, 1H), 8.00 (s, 1H), 7.93 (d, J = 8.2 Hz, 2H), 7.79 (d, J = 8.2 Hz, 2H), 4.63 (t, J = 18.9 Hz, 1H). ^{13}C NMR (126 MHz, D_2O): δ 163.6, 156.3, 153.9, 137.5, 136.7, 129.2 (q, J = 32.4 Hz), 126.2, 126.0 (q, J = 3.8 Hz), 124.1 (q, J = 270.1 Hz), 118.5, 116.5, Cα observed by HSQC. HSQC (^{1}H−^{13}C): ^{1}H δ 4.63 correlates with ^{13}C δ 51.1. ^{31}P NMR (81 MHz, D_2O): δ 13.6. HRMS (ESI−) calculated for $C_{14}H_{11}F_3N_3P_2O_6S$ m/z [M − H]$^-$, 467.97959; found, m/z 467.9783.

*(((6-(3-(Trifluoromethyl)phenyl)thieno[2,3-d]pyrimidin-4-yl)-amino)methylene)diphosphonic Acid (**6i**).* Isolated as a white solid, 23.4 mg (44% overall isolated yield). ^{1}H NMR (500 MHz, D_2O): δ 8.29 (s, 1H), 8.08 (s, 1H), 8.00 (d, J = 7.8 Hz, 1H), 7.95 (s, 1H), 7.71 (d, J = 7.8 Hz, 1H), 7.65 (t, J = 7.8 Hz, 1H), 4.64 (t, J = 18.8 Hz, 1H). ^{13}C NMR (126 MHz, D_2O): δ 163.5, 156.3, 153.8, 137.7, 134.0, 130.8 (q, J = 32.9 Hz), 129.7, 129.5, 124.9 (q, J = 3.7 Hz), 123.9 (q, J = 272.3 Hz), 122.7 (q, J = 3.8 Hz), 118.5, 115.9, 50.9. ^{31}P NMR (81 MHz, D_2O): δ 13.7. HRMS (ESI−) calculated for $C_{14}H_{11}F_3N_3P_2O_6S$ m/z [M − H]$^-$, 467.98014; found, m/z 467.978033.

*(((6-(4-Methoxyphenyl)thieno[2,3-d]pyrimidin-4-yl)amino)-methylene)diphosphonic Acid (**6j**).* Isolated as a pale-yellow powder; 30.8 mg (71% overall isolated yield). ^{1}H NMR (400 MHz, D_2O): δ 8.11 (s, 1H), 7.58(s, 1H), 7.57 (d, J = 8.0 Hz, 2H), 6.91 (d, J = 8.0 Hz, 2H), 3.70 (s, 3H); central methylene proton obscured by solvent signal. ^{13}C NMR (126 MHz, D_2O): δ 162.7, 159.2, 156.0, 153.2, 139.1, 127.5, 126.3, 118.7, 114.6, 113.4, 55.3, Cα observed by HSQC. HSQC (^{1}H−^{13}C): ^{1}H δ 4.74 correlates with ^{13}C δ 49.0. ^{31}P NMR (81 MHz, D_2O): δ 13.7. HRMS (ESI−) calculated for $C_{14}H_{14}N_3P_2O_7S$ m/z [M − H]$^-$, 430.00332; found, m/z 430.00442.

*(((6-(4-Isopropoxyphenyl)thieno[2,3-d]pyrimidin-4-yl)amino)-methylene)diphosphonic Acid (**6k**).* Isolated as a white powder; 21.9 mg (54% overall isolated yield). ^{1}H NMR (500 MHz, D_2O): δ 8.17 (s, 1H), 7.69 (s, 1H), 7.67 (d, J = 8.8 Hz, 2H), 7.02 (d, J = 8.8 Hz, 2H), 1.27 (d, J = 6.1, 6H); central methylene proton and I-Pr-CH obscured by solvent signal. ^{13}C NMR (126 MHz, D_2O): δ 164.4, 158.9, 157.7, 155.0, 140.7, 129.2, 128.2, 120.4, 118.6, 115.3, 73.3, 22.7, Cα observed by HSQC. HSQC (^{1}H−^{13}C): ^{1}H δ 4.60 correlates with ^{13}C δ 73.3 and ^{1}H δ 4.47 correlates with ^{13}C δ 50.4. ^{31}P NMR (81 MHz, D_2O): δ 13.7. HRMS (ESI−) calculated for $C_{16}H_{18}N_3P_2O_7S$ m/z [M − H]$^-$, 458.03462; found, m/z 458.03532.

*(((6-(4-Cyclopropoxyphenyl)thieno[2,3-d]pyrimidin-4-yl)amino)-methylene)diphosphonic Acid (**6l**).* Isolated as a beige powder; 16.2 mg (38% overall isolated yield). ^{1}H NMR (500 MHz, D_2O): δ 8.12 (s, 1H), 7.63 (s, 1H), 7.62 (d, J = 8.7 Hz, 2H), 7.10 (d, J = 8.7 Hz, 2H), 4.42 (br s, 1H), 3.82−3.80 (m, 1H), 0.74−0.71 (m, 2H), 0.65−0.62 (m, 2H); central methylene proton obscured by solvent signal. ^{13}C NMR (126 MHz, D_2O): δ 162.7, 158.5, 156.0, 153.3, 139.1, 127.4, 126.7, 118.7, 115.7, 113.6, 51.3, 5.45, Cα observed by HSQC at ∼50. ^{31}P NMR (81 MHz, D_2O): δ13.6. HRMS (ESI−) calculated for $C_{16}H_{16}N_3P_2O_7S$ m/z [M − H]$^-$, 456.0190; found, m/z 456.0189.

*(((6-(4-Cyclopropylphenyl)thieno[2,3-d]pyrimidin-4-yl)amino)-methylene)diphosphonic Acid (**6m**).* Isolated as a light-brown powder 18.8 mg (47% overall isolated yield). ^{1}H NMR (400 MHz, D_2O): δ 8.13(s, 1H), 7.70 (s, 1H), 7.58 (d, J = 8.3 Hz, 2H), 7.11 (d, J = 8.3 Hz, 2H), 4.46 (t, J = 18.7 Hz, 1H), 1.88−1.84 (m, 1H), 0.93−0.86 (m, 2H), 0.66−0.62 (m, 2H). ^{13}C NMR (75 MHz, D_2O): δ 165.4, 158.7, 156.0, 148.0, 141.8, 132.9, 128.7, 128.6, 121.2, 116.6, 17.1, 11.9, Cα observed by HSQC. HSQC (^{1}H−^{13}C): ^{1}H δ 4.46 correlates with ^{13}C δ 50.9. ^{31}P NMR (81 MHz, D_2O): δ 13.8. HRMS (ESI−) calculated for $C_{16}H_{16}N_3P_2O_6S$ m/z [M − H]$^-$, 440.02405; found, m/z 440.02414.

*(((6-(4-(2,2-Difluorocyclopropyl)phenyl)thieno[2,3-d]pyrimidin-4-yl)amino)methylene)diphosphonic Acid (**6n**).* Isolated as a pale-yellow solid 26.7 mg (50% overall isolated yield). ^{1}H NMR (500 MHz, D_2O): δ 8.27 (s, 1H), 7.86 (s, 1H), 7.75 (d, J = 8.4 Hz, 2H), 7.38 (d, J = 8.4 Hz, 2H), 4.63 (t, J = 18.9 Hz, 1H), 2.98−2.91 (m, 1H), 1.96−1.90 (m, 1H), 1.86−1.78 (m, 1H). ^{13}C NMR (126 MHz, D_2O): δ 163.2, 156.2, 153.4, 138.9, 134.3, 132.0, 128.7, 126.0, 118.5, 115.6, 113.3 (t, J = 285 Hz), 26.38 (t, J = 11.2 Hz), 16.1 (t, J = 10.3 Hz), Cα observed by HSQC. HSQC (^{1}H−^{13}C): ^{1}H δ 4.63 correlates with ^{13}C δ 50.5. ^{31}P NMR (81 MHz, D_2O): δ 13.7. HRMS (ESI−) calculated for $C_{16}H_{14}F_2N_3P_2O_6S$ m/z [M − H]$^-$, 476.0052; found, m/z 476.0046.

In Vitro Inhibition Assays. The in vitro enzymatic assay of method 1 (M1) was carried out as previously described.[11,14,16] The human FPPS in vitro inhibition assay of method 2 (M2) was carried out using 4 ng of the human recombinant FPPS and 0.2 μM of each substrates, GPP and IPP (^{3}H-IPP, 3.33 mCi/mmol) in a final volume of 100 μL of buffer containing 50 mM Tris pH 7.7, 1 mM $MgCl_2$, 0.5 mM TCEP, 20 μg/mL BSA, and 0.01% Triton X-100. All assays were run in triplicate with a 10 min preincubation period; hFPPS and inhibitor were incubated in the assay buffer in a volume of 80 μL at 37 °C for 10 min. After the 10 min preincubation, the substrates were added to the reaction mixture (bringing the inhibitor and substrates to the desired final concentrations). All assays were incubated at 37 °C for 8 min and terminated by the addition of 200 μL of HCl/methanol (1:4), followed by an additional incubation of 10 min at 37 °C. The assay mixture was then extracted with 700 μL of ligroin, dried through a plug of anhydrous $MgSO_4$, and 300 μL of the ligroin phase was combined with 8 mL of scintillation cocktail. The radioactivity was then counted using a Beckman Coulter LS6500 liquid scintillation counter.

Reagents for in Vitro Assay. The hFFPS enzyme was stored at −80 °C as a 2 μg/μL solution in the eluent buffer (50 mM HEPES pH 7.5, 500 mM NaCl, 250 mM imidazole, 5% glycerol, 0.5 mM TCEP). ^{3}H-IPP was purchased from American Radiolabeled Chemicals (ART 0377A: 1mCi/mL, 60 Ci/mmol in 0.1 M Tris pH 7.5) and was diluted with cold IPP to a specific activity of 33 mCi/mmol and 2 μM concentration in 200 mM Tris pH 7.7; the IPP solution was stored at −10 °C, warmed to 0 °C, and kept on ice during assay setup. Unlabeled IPP and GPP were purchased from Isoprenoids, Lc. as their ammonium salts. GPP was dissolved and diluted to a 2 μM concentration in 200 mM Tris pH 7.7. It was stored at −10 °C, warmed to 0 °C, and kept on ice during assay setup. Ligroin was

dx.doi.org/10.1021/jm400946f | J. Med. Chem. 2013, 56, 7939−7950

purchased from Sigma Aldrich, liquid scintillation cocktail was purchased from MP Biomedicals: Ecolite (no. 882475),

Cell Culture and Viability Assays. The RPMI 8226 multiple myeloma cell line was obtained courtesy of Dr. Leif Bergsagel (Mayo Clinic, Scottsdale, AZ) and cultured in RPMI-1640 medium supplemented with 10% fetal bovine serum (Gibco BRL, Gaithesburg, MD) supplemented with 2 mM L-glutamine in a 5% CO_2 atmosphere at 37 °C. A dilution method was used to determine EC_{50} values for inhibition for each target compound; compounds were diluted in culture medium. Cells were seeded in 96-well plates at a density 10000 cells per well incubated for 2 h before the addition of 10 μL of compound at half-logarithmic dilutions from 100 nM to 333 μM with a fixed final volume. Plates were then incubated for 72 h at 37 °C in the presence 5% CO_2, following which an MTT, 4,5-dimethylthiazole-2-yl)-2,5-diphenyltetrazolium bromide reagent was used according to the manufacturers documentation (Promega, Madison, WI). Plates were read at OD490 nM on a Dynex MRX microplate reader (Magellan Biosciences, Chelmsford MA). Results were analyzed to obtain dose–response curves and EC_{50} calculations using GraphPad PRISM version 5 (GraphPad Software, San Diego, CA).

Calculation of CLogP Values. CLogP values were estimated using the CLogP tool in ChemDraw Ultra 12.0; the two phosphonate moieties were deleted from each structure in order to simplify the calculations. For example, the structures of **2a** and **6m** used for the calculations are shown below as fragment **2a–x** and **6m–x**, respectively. Good correlation was observed between the CLogP values of known compounds calculated using the same tool and those reported in the literature (predicted by other in silico tools, such as MedChem Studio prediction software; ADMET Predictor 5.5, Simulation Plus Inc.). IC_{50} values not determined (nd).

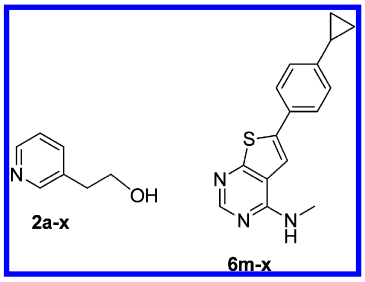

Crystallization of hFPPS in Complex with Inhibitors 6f and 6m. Compounds **6f** and **6m** were prepared as 20 mM stock solutions in 100 mM TrisHCl (pH 7.5). Each stock solution was added to the concentrated hFPPS sample to give the final concentrations of 1 mM inhibitor and 0.25 mM protein (10 mg/mL). To obtain crystals suitable for X-ray diffraction analysis, microseeding was employed. All crystals were grown at 22 °C by vapor diffusion in sitting drops composed of 1 μL of protein/inhibitor mixture and 1 μL of crystallization solution, and additional 0.5 μL of seed solution when added. Seed solutions were prepared by using Seed Bead kits (Hampton Research). For the hFPPS–CL01–121 complex, the initial crystals formed in a crystallization solution composed of 0.1 M TrisHCl (pH 8.5) and 2 M ammonium dihydrogen phosphate. In the first round of seeding optimization, crystals of improved quality grew in a new crystallization solution containing 0.09 M sodium acetate (pH 4.6), 0.17 M ammonium sulfate, 1.5 mM magnesium chloride, 25.5% (w/v) PEG MME 2000, and 15% (v/v) glycerol. Diffraction quality crystals were identified in the second round of optimization in yet another crystallization condition consisting of 0.1 M TrisHCl (pH 7.0), 0.25 M magnesium chloride, and 7% (w/v) PEG 8000. For the hFPPS–CL02–134 complex, crystals were grown in a solution composed of 0.08 M sodium cacodylate (pH 6.5), 0.16 M magnesium acetate, 16% (w/v) PEG 8000, and 20% glycerol, by using the hFPPS–CL01–121 cocrystals as heterogeneous seeds.

Data Collection, Processing, and Structure Refinement. Diffraction data were collected from single crystals at 100K with synchrotron radiation (Canadian Light Source, Saskatoon, SK) and a Rayonix MX300 CCD detector. The diffraction data were indexed and scaled with either HKL2000[66] or the *xia2* package.[67] The initial structure models were built by difference Fourier methods with a ligand/solvent-omitted input model generated from the PDB model 4H5D. The initial models were further improved through iterative rounds of manual and automated refinement with COOT[68] and REFMAC5.[69] The final models have been deposited into the Protein Data Bank. Data collection and refinement statistics, as well as the PDB IDs for these models, are presented in Table 3.

■ ASSOCIATED CONTENT

Ⓢ Supporting Information

NMR spectra of final inhibitors **6a–n**; examples of homogeneity data for key final inhibitors at (bisphosphonic acids). Some experimental details on the dynamic light scattering (DSL) studies. This material is available free of charge via the Internet at http://pubs.acs.org.

■ AUTHOR INFORMATION

Corresponding Author

*Phone: 514-398-3638. Fax: 514-398-3797. Email: Youla.tsantrizos@mcgill.ca.

Notes

The authors declare no competing financial interest.

■ ACKNOWLEDGMENTS

^{1}H NMR experiments to assess HAP binding of our inhibitors were acquired on a 500 MHz NMR instrument at the Québec/Eastern Canada High Field NMR Facility, supported by the Natural Sciences and Engineering Research Council of Canada (NSERC), the Canada Foundation for Innovation (CFI), the Québec Ministère de la Recherche en Science et Technologie (FQRNT), and McGill University. We are grateful Xian Fang Huang for assistance with the cell-based assays. We also thank to Jinming Guan for her help with the preparation of some compounds. Financial support for this work was provided by NSERC and FQRNT (research grants to Y. S. Tsantrizos) and the Canadian Institute of Health Research (CIHR; research grants to A. M. Berghuis and M. Sebag).

■ ABBREVIATIONS USED

hFPPS, human farnesyl pyrophosphate synthase; hGGPPS, human geranylgeranyl pyrophosphate synthase; DMAPP, dimethylallyl pyrophosphate; IPP, isopentenyl pyrophosphate; GPP, geranyl pyrophosphate; FPP, farnesyl pyrophosphate; GGPP, geranylgeranyl pyrophosphate; *N*-BPs, nitrogen-containing bisphosphonates; MM, multiple myeloma; GTPases, small guanine triphosphate binding proteins; ANT, mitochondrial adenine nucleotide translocase; IFNγ, interferon-γ; TNFα, tumor necrosis factor-α; hSQS, human squalene synthase; ApppI, derivative 1-adenosin-5′-yl ester 3-(3-methylbut-3-enyl) triphosphoric acid; HAP, hydroxyapatite; SAS, structure–activity studies; SAR, structure–activity relationship; DLS, dynamic light scattering

■ REFERENCES

(1) Dunford, J. E.; Thompson, K.; Coxon, F. P.; Luckma, S. P.; Hahn, F. M.; Poulter, C. D.; Ebetino, F. H.; Rogers, M. J. Structure–Activity Relationship for Inhibition of Farnesyl Diphosphate Synthase in Vitro and Inhibition of Bone Resorption in Vivo by Nitrogen-Containing Bisphosphonates. *J. Pharmacol. Exp. Ther.* **2001**, *296*, 235–242.

(2) Coxon, F. P.; Thompson, K.; Rogers, M. J. Recent advances in understanding the mechanism of action of bisphosphonates. *Curr. Opin. Pharmacol.* **2006**, *6*, 307–312.

(3) Chapman, M. A.; Lawrence, M. S.; Keats, J. J.; Cibulskis, K.; Sougnez, C.; Schinzel, A. C.; Harview, C. L.; Brunet, J. P.; Ahmann, G. J.; Adli, M.; Anderson, K. C.; Ardlie, K. G.; Auclair, D.; Baker, A.; Bergsagel, P. L.; Bernstein, B. E.; Drier, Y.; Fonseca, R.; Gabriel, S. B.; Hofmeister, C. C.; Jagannath, S.; Jakubowiak, A. J.; Krishnan, A.; Levy, J.; Liefeld, T.; Lonial, S.; Mahan, S.; Mfuko, B.; Monti, S.; Perkins, L. M.; Onofrio, R.; Pugh, T. J.; Rajkumar, S. V.; Ramos, A. H.; Siegel, D. S.; Sivachenko, A.; Stewart, A. K.; Trudel, S.; Vij, R.; Voet, D.; Winckler, W.; Zimmerman, T.; Carpten, J.; Trent, J.; Hahn, W. C.; Garraway, L. A.; Meyerson, M.; Lander, E. S.; Getz, G.; Golub, T. R. Initial genome sequencing and analysis of multiple myeloma. *Nature* **2011**, *471*, 467−472.

(4) Coleman, R. E. Clinical Features of Metastatic Bone Disease and Risk of Skeletal Morbidity. *Clin. Cancer Res.* **2006**, *12*, 6243s−6249s.

(5) Fournier, P. G.; Stresing, V.; Ebetino, F. H.; Clézardin, P. How do Bisphosphonates Inhibit Bone Metastasis in Vivo. *Neoplasia* **2010**, *12*, 571−578.

(6) Mönkkönen, H.; Auriola, S.; Lehenkari, P.; Kellinsalmi, M.; Hassinen, I. E.; Vepsäläinen, J.; Mönkkönen, J. A new endogenous ATP analog (ApppI) inhibits the mitochondrial adenine nucleotide translocase (ANT) and is responsible for the apoptosis induced by nitrogen-containing bisphosphonates. *Br. J. Pharmacol.* **2006**, *147*, 437−445.

(7) Mitrofan, L. M.; Pelkonen, J.; Mönkkönen, J. The level ofATP analogs and isopentenyl pyrophosphate correlates with zoledronic acid-induced apoptosis in cancer cells in vitro. *Bone* **2009**, *45*, 1153−1160.

(8) Morita, C. T.; Jin, C.; Sarikonda, G.; Wang, H. Nonpeptide antigens, presentation mechanisms, and immunological memory of human Vg2Vg2 T cells: discriminating friends from foe through the recognition of prenyl pyrophosphate antigens. *Immunol. Rev.* **2007**, *215*, 59−76.

(9) Tong, H.; Kuder, C. H.; Wasko, B. M.; Hohl, R. J. Quantitative determination of isopentenyl diphosphate in cultured mammalian cells. *Anal. Biochem.* **2013**, *433*, 36−42.

(10) Rondeau, J.-M.; Bitsch, F.; Bourgier, E.; Geiser, M.; Hemmig, R.; Kroemer, M.; Lehmann, S.; Ramage, P.; Rieffel, S.; Strauss, A.; Green, J. R.; Jahnke, W. Structural Basis for the Exceptional in vivo Efficacy of Bisphosphonate Drugs. *ChemMedChem* **2006**, *1*, 267−273.

(11) Kavanagh, K. L.; Guo, K.; Dunford, J. E.; Wu, X.; Knapp, S.; Ebetino, F. H.; Rogers, M. J.; Russell, R. G. G.; Oppermann, U. The molecular mechanism of nitrogen-containing bisphosphonates as antiosteoporosis drugs. *Proc. Natl. Acad. Sci. U. S. A.* **2006**, *103*, 7829−7834.

(12) Martin, M. B.; Arnold, W.; Heath, H. T., III; Urbina, J. A.; Oldfield, E. Nitrogen-Containing Bisphosphonates as Carbocation Transition State Analogs for Isoprenoid Biosynthesis. *Biochem. Biophys. Res. Commun.* **1999**, *263*, 754−758.

(13) Marma, M. S.; Xia, Z.; Stewart, C.; Coxon, F.; Dunford, J. E.; Baron, R.; Kashemirov, B. A.; Ebetino, F. H.; Triffitt, J. T.; Russell, G. G.; McKenna, C. E. Synthesis and Biological Evaluation of α-Halogenated Bisphosphonate and Phosphonocarboxylate Analogues of Risedronate. *J. Med. Chem.* **2007**, *50*, 5967−5975.

(14) Fournier, P. G.; Stresing, V.; Ebetino, F. H.; Clézardin, P. How Do Bisphosphonates Inhibit Bone Metastasis In Vivo? *Neoplasia* **2010**, *12*, 571−578.

(15) Drake, M. T.; Cremers, S. C. L. M. Bisposphonate Therapeutics in Bone Diseases: The Hard and Soft Data on Osteoclast Inhibition. *Mol. Interventions* **2010**, *10*, 141−152.

(16) Russell, R. G. G.; Xia, Z.; Dunford, J. E.; Oppermann, U.; Kwaasi, A.; Hulley, P. A.; Kavanagh, K. L.; Triffitt, J. T.; Lundy, M. W.; Phipps, R. J.; Barnett, B. L.; Coxon, F. P.; Rogers, M. J.; Watts, N. B.; Ebetino, F. H. Bisphosphonates. An Update on Mechanism of action and How These Relate to Clinical Efficacy. *Ann. N. Y. Acad. Sci.* **2007**, *1117*, 209−257.

(17) Frost, M. L.; Siddique, M.; Blake, G. M.; Moore, A. E.; Marsden, P. K.; Schleyer, P. J.; Eastell, R.; Fogelman, I. Regional bone metabolism at the lumbar spine and hip following discontinuation of alendronate and risedronate treatment in postmenopausal women. *Osteoporos Int.* **2012**, *23*, 2107−2116.

(18) Grey, A.; Bolland, M. J.; Wattie, D.; Horne, A.; Gamble, G.; Reid, I. R. The antiresorptive effects of a single dose of zoledronate persists for two years: a randomized placebo-control trial in osteopenic postmenopausal women. *J. Clin. Endocrinol. Metab.* **2009**, *94*, 538−544.

(19) Eastell, R.; Walsh, J. S.; Watts, N. B.; Siris, E. Bisphosphonates for postmenopausal osteoporosis. *Bone* **2011**, *49*, 82−88.

(20) Skerjanec, A.; Berenson, J.; Hsu, C.; Major, P.; Miller, W. H., Jr.; Ravera, C.; Schran, H.; Seaman, J.; Waldmeier, F. The pharmacokinetics and pharmacodynamics of zoledronic acid in cancer patients with varying degrees of renal function. *J. Clin. Pharmacol.* **2003**, *43*, 154−162.

(21) Weiss, H. M.; Pfaar, U.; Schweitzer, A.; Wiegand, H.; Skerjanec, A.; Schran, H. Biodistribution and plasma protein binding of zoledronic acid. *Drug Metab. Dispos.* **2008**, *36*, 2043−2049.

(22) Morgan, G. J.; Davies, F. E.; Gregory, W. M.; Cocks, K.; Bell, S. E.; Szubert, A. J.; Navarro-Coy, N.; Drayson, M. T.; Owen, R. G.; Feyler, S.; Ashcroft, A. J.; Ross, F.; Byrne, J.; Roddie, H.; Rudin, C.; Cook, G.; Jackson, G. H.; Child, J. A. First-line treatment with zoledronic acid as compared with clodronic acid in multiple myeloma (MRC Myeloma IX): a randomized controlled trial. *Lancet* **2010**, *376*, 1989−1999.

(23) Morgan, G. J.; Davies, F. E.; Gregory, W. M.; Szubert, A. J.; Bell, S. E.; Drayson, M. T.; Owen, R. G.; Ashcroft, A. J.; Jackson, G. H.; Child, J. A. Effects of induction and maintenance plus long-term bisphosphonates on bone disease in patients with multiple myeloma: the Medical Research Council Myeloma IX Trial. *Blood* **2012**, *119*, 5374−5383.

(24) Gnant, M.; Mlineritsch, B.; Schippinger, W.; Luschin-Ebengreuth, G.; Pöstlberger, S.; Menzel, C.; Jakesz, R.; Seifert, M.; Hubalek, M.; Bjelic-Radisic, V.; Samonigg, H.; Tausch, C.; Eidtmann, H.; Steger, G.; Kwasny, W.; Dubsky, P.; Fridrik, M.; Fitzal, F.; Stierer, M.; Rücklinger, E.; Greil, R. Endocrine Therapy plus Zoledronic Acid in Premenopausal Breast Cancer. *New Engl. J. Med.* **2009**, *360*, 679−691.

(25) Coleman, R. E.; Marshall, H.; Cameron, D.; Dodwell, D.; Burkinshaw, R.; Keane, M.; Gil, M.; Houston, S. J.; Grieve, R. J.; Barrett-Lee, P. J.; Ritchie, D.; Pugh, J.; Gaunt, C.; Rea, U.; Peterson, J.; Davies, C.; Hiley, V.; Gregory, W.; Bell, R. Breast-Cancer Adjuvant Therapy with Zoledronic Acid. *New Engl. J. Med.* **2011**, *365*, 1396−1405.

(26) Leung, C.-Y.; Langille, A. M.; Mancuso, J.; Tsantrizos, Y. S. Discovery of Thienopyrimidine-Based Inhibitors of the Human Farnesyl Pyrophosphate Synthase—Parallel Synthesis of Analogs via a Trimethylsilyl Ylidene Intermediate. *Bioorg. Med. Chem. Lett.* **2013**, *21*, 2229−2240.

(27) Tani, N.; Rahnasto-Rilla, M.; Wittekindt, C.; Salminen, K. A.; Ritvanen, A.; Ollakka, R.; Koskiranta, J.; Raunio, H.; Juvonen, R. O. Antifungal activity of novel non-azole molecules against *S. cerevisiae* and *C. albicans*. *Eur. J. Med. Chem.* **2012**, *47*, 270−277.

(28) Babu, Y.; Chand, P.; Wu, M.; Kotian, P. L.; Kumar, V. S.; Lin, T.-H.; El-Kattan, Y.; Ghosh, A. K. Therapeutic Furopyrimidines and Thienopyrimidines. WO 2006/050161, 2006.

(29) McClellan, W. J.; Dai, Y.; Abad-Zapatero, C.; Albert, D. H.; Bouska, J. J.; Glaser, K. B.; Magoc, T. J.; Marcotte, P. A.; Osterling, D. J.; Stewart, K. D.; Davidsen, S. K.; Michaelides, M. R. Discovery of potent and selective thienopyrimidine inhibitors of Aurora kinases. *Bioorg. Med. Chem. Lett.* **2011**, *21*, 5620−5624.

(30) Dai, Y.; Guo, Y.; Frey, R. R.; Ji, Z.; Curtin, M. L.; Ahmed, A. A.; Albert, D. H.; Arnold, L.; Arries, S. S.; Barlozzari, T.; Bauch, J. L.; Bouska, J. J.; Bousquet, P. F.; Cunha, G. A.; Glaser, K. B.; Guo, J.; Li, J.; Marcotte, P. A.; Marsh, K. C.; Moskey, M. D.; Pease, L. J.; Stewart, K. D.; Stoll, V. S.; Tapang, P.; Wishart, N.; Davidsen, S. K.; Michaelides, M. R. Thienopyrimidine Ureas as Novel and Potent Multitargeted Receptor Tyrosine Kinase Inhibitors. *J. Med. Chem.* **2005**, *48*, 6066−6083.

(31) Luke, R. W.; Ballard, P.; Buttar, D.; Campbell, L.; Curwen, J.; Emery, S. C.; Griffen, A. M.; Hassall, L.; Hayter, B. R.; Jones, C. D.; McCoull, W.; Mellor, M.; Swain, M. L.; Tucker, J. A. Novel thienopyrimidine and thiazolopyrimidine kinase inhibitors with activity against Tie-2 in vitro and in vivo. *Bioorg. Med. Chem. Lett.* **2009**, *19*, 6670−6674.
(32) Horiuchi, T.; Chiba, J.; Uoto, K.; Soga, T. Discovery of novel thieno[2,3-*d*]pyrimidin-4-yl hydrazine-based inhibitors of cyclin D1-CDK4: synthesis, biological evaluation, and structure−activity relationship. *Bioorg. Med. Chem. Lett.* **2009**, *19*, 305−308.
(33) Axten, J. M.; Grant, S. W.; Heerding, D. A.; Medina, J. R.; Romeril, S. P.; Tang, J. Chemical Compounds. WO 2011/119663, 2011.
(34) Edgar, K. A.; Wallin, J. J.; Berry, M.; Lee, L. B.; Prior, W. W.; Sampath, D.; Friedman, L. S.; Belvin, M. Isoform-Specific Phosphoinositide 3-Kinase Inhibitors Exert Distinct Effects in Solid Tumors. *Cancer Res.* **2010**, *70*, 1164−1172.
(35) Heffron, T. P.; Wei, B. Q.; Olivero, A.; Staben, S. T.; Tsui, V.; Do, S.; Dotson, J.; Folkes, A. J.; Goldsmith, P.; Goldsmith, R.; Gunzner, J.; Lesnick, J.; Lewis, C.; Mathieu, S.; Nonomiya, J.; Shuttleworth, S.; Sutherlin, D. P.; Wan, N. C.; Wang, S.; Wiesmann, C.; Zhu, B.-Y. Rational Design of Phosphoinositide 3-Kinase α Inhibitors That Exhibit Selectivity over the Phosphonoinositide 3-Kinase β Isoform. *J. Med. Chem.* **2011**, *54*, 7815−7833.
(36) Rheault, T. R.; Ceferro, T. R.; Dickerson, S. H.; Donaldson, K. H.; Gaul, M. D.; Goetz, A. S.; Mullin, R. J.; McDonald, O. B.; Petrov, K. G.; Rusnak, D. W.; Shewchuk, L. M.; Spehar, G. M.; Truesdale, A. T.; Vanderwall, D. E.; Wood, E. R.; Uehling, D. E. Thienopyrimidine-based dual EGFR/ErbB-2 inhibitors. *Bioorg. Med. Chem. Lett.* **2009**, *19*, 817−820.
(37) Lin, Y.-S.; Park, J.; De Schutter, J. W.; Huang, X. F.; Berghuis, A. M.; Sebag, M.; Tsantrizos, Y. S. Design and Synthesis of Active Site Inhibitors of the Human Farnesyl Pyrophosphate Synthase—Apoptosis and Inhibition of ERK Phosphorylation in Multiple Myeloma Cells. *J. Med. Chem.* **2012**, *55*, 3201.
(38) De Schutter, J. W.; Shaw, J.; Lin, Y.-S.; Tsantrizos, Y. S. Design of Potent Bisphosphonate Inhibitors of the Human Farnesyl Pyrophosphate Synthase via Targeted Interactions with the Active Site "Capping" Phenyls. *Bioorg. Med. Chem.* **2012**, *20*, 5583−5591.
(39) Hesse, S.; Perspicace, E.; Kirsch, G. Microwave-assisted synthesis of 2-aminothiophene-3-carboxylic acid derivatives, 3*H*-thieno[2,3-*d*]pyrimidin-4-one and 4-chlorothieno[2,3-*d*]pyrimidine. *Tetrahedron Lett.* **2007**, *48*, 5261−5264.
(40) Tranberg, C. E.; Zickgraf, A.; Giunta, B. N.; Luetjens, H.; Figler, H.; Murphree, L. J.; Falke, R.; Fleischer, H.; Linden, J.; Scammells, P. J.; Olsson, R. A. 2-Amino-3-aroyl-4,5-alkylthiophenes: Agonist Allosteric Enhancers at Human A_1 Adenosine Receptors. *J. Med. Chem.* **2002**, *45*, 382−389.
(41) Eckert, G. P.; Hooff, G. P.; Strandjord, D. M.; Igbavboa, U.; Volmer, D. A.; Müller, W. E.; Wood, W. G. Regulation of the brain isoprenoids farnesyl- and geranylgeranylpyrophosphate is altered in male Alzheimer patients. *Neurobiol. Dis.* **2009**, *35*, 251−257.
(42) Hooff, G. P.; Wood, W. G.; Müller, W. E.; Eckert, G. P. Isoprenoids, small GTPases and Alzheimer's diseases. *Biochim. Biophys. Acta* **2010**, *1801*, 896−905.
(43) Zhang, Y.; Leon, A.; Song, Y.; Studer, D.; Haase, C.; Koscielski, L. A.; Oldfield, E. Activity of Nitrogen-Containing and Non-Nitrogen-Containing Bisphosphonates on Tumor Cell Lines. *J. Med. Chem.* **2006**, *49*, 5804−5814.
(44) Ezra, A.; Hoffma, A.; Breuer, E.; Alferiev, I. S.; Mönkkönen, J.; Hanany-Rozen, N.El; Weiss, G.; Stepensky, D.; Gati, I.; Cohen, H.; Törmä, S.; Amidon, G. L.; Golomb, G. A Peptide Prodrug Approach for Improving Bisphosphonate Oral Absorption. *J. Med. Chem.* **2000**, *43*, 3641−3652.
(45) Shmeeda, H.; Amitay, Y.; Gorin, J.; Tsemach, D.; Mak, L.; Ogorka, J.; Kumar, S.; Zhang, J. A.; Gabizon, A. Delivery of zoledronic acid encapsulated in folate-targeted liposome results in potent in vitro cytotoxic activity on tumor cells. *J. Controlled Release* **2010**, *146*, 76−83.
(46) Zhang, Y.; Cao, R.; Yin, F.; Hudock, M. P.; Guo, R.-T.; Krysiak, K.; Mukherjee, S.; Gao, Y.-G.; Robinson, H.; Song, Y.; No, J. H.; Bergan, K.; Leon, A.; Cass, L.; Goddard, A.; Chang, T.-K.; Lin, F.-Y.; Van Beek, E.; Papapoulos, S.; Wang, A.H.-J.; Kubo, T.; Ochi, M.; Mukkamala, D.; Oldfield, E. Lipophilic Bisphosphonates as Dual Farnesyl/Geranylgeranyl Diphosphate Synthase Inhibitors: An X-ray and NMR Investigation. *J. Am. Chem. Soc.* **2009**, *131*, 5153−5162.
(47) Zhang, Y.; Cao, R.; Yin, F.; Lin, F.-Y.; Wang, H.; Krysiak, K.; No, J.-H.; Mukkamala, D.; Houlihan, K.; Li, J.; Morita, C. T.; Oldfield, E. Lipophilic Pyridinium Bisphosphonates: Potent gd T Cell Stimulators. *Angrew. Chem. Int. Ed.* **2010**, *49*, 1136−1138.
(48) Simoni, D.; Gebbia, N.; Invidiata, F. P.; Eleopra, M.; Marchetti, P.; Rondanin, R.; Baruchello, R.; Provera, S.; Marchioro, C.; Tolomeo, M.; Marinelli, L.; Limongelli, V.; Novellino, E.; Kwaasi, A.; Dunford, J.; Buccheri, S.; Caccamo, N.; Dieli, F. Design, Synthesis, and Biological Evaluation of Novel Aminobisphosphonates Possessing an in Vivo Antitumor Activity Through a gd-T Lymphocyte-Mediated Activation Mechanism. *J. Med. Chem.* **2008**, *51*, 6800−6807.
(49) Ebetino, F. H.; Mazur, A.; Lundy, M. W.; Russeli, R. G. G. 4-Azaindole Bisphosphonates. WO 2010/033980 A2, 2010.
(50) Ebetino, F. H.; Mazur, A.; Lundy, M. W.; Russeli, R. G. G. 5-Azaindole Bisphosphonates. WO 2010/033981 A2, 2010.
(51) Reed, B. C.; Rilling, H. C. Crystallization and partial characterization of prenyltransferase from avian liver. *Biochemistry* **1975**, *14*, 50−54.
(52) Glickman, J. F.; Schmid, A. Farnesyl Pyrophosphate Synthase: Real-Time Kinetics and Inhibition by Nitrogen-Containing Bisphosphonates in a Scintillation Assay. *Assay Drug Dev. Technol.* **2007**, *5*, 205−214.
(53) Dunford, J. E.; Kwaasi, A. A.; Rogers, M. J.; Barnett, B. L.; Ebetino, F. H.; Russell, R. G. G.; Oppermann, U.; Kavanagh, K. L. Structure−Activity Relationship Among the Nitrogen Containing Bisphosphonates in Clinical Use and Other Analogues: Time-Dependent Inhibition of Human Farnesyl Pyrophosphate Synthase. *J. Med. Chem.* **2008**, *51*, 2187−2195.
(54) Amstutz, R.; Bold, G.; Cotesta, S.; Jahnke, W.; Marzinzik, A.; Mueller-Hartwieg, C.; Ofner, S.; Stauffer, F.; Zimmermann, J. Quinolines as Inhibitors of Farnesyl Pyrophosphate Synthase. WO 2009/106586 A1, 2009.
(55) Owen, S. C.; Doak, A. K.; Wassam, P.; Shoichet, M. S.; Schoichet, B. K. Colloidal Aggregation Affects the Efficacy of Anticancer Drugs in Cell Culture. *ACS Chem. Biol.* **2012**, *7*, 1429−1435.
(56) Giger, E. V.; Castagner, B.; Leroux, J.-C. Biomedical applications of bisphosphonates. *J. Controlled Release* **2013**, *167*, 175−188.
(57) Freire, E.; Vega, D. R.; Baggio, R. Zoledronate complexes. III. Two zoledronate complexes with alkaline earth metals: $[Mg(C_5H_9N_2O_7P_2)_2(H_2O)_2]$ and $[Ca(C_5H_8N_2O_7P_2)(H_2O)]_n$. *Acta Crystallogr., Sect. C: Cryst. Struct. Commun.* **2010**, *C66*, m166−m170.
(58) Kunnas-Hiltunen, S.; Matilainen, M.; Vepsäläinen, J. J.; Ahlgrén, M. X-ray diffraction study of bisphosphonate metal complexes: Mg, Sr and Ba complexes of (dichloromethylene)bispho-sphonic acid *P,P'*-dibenzoyl anhydride. *Polyhedron* **2009**, *28*, 200−204.
(59) Peukert, S.; Sun, Y.; Zhang, R.; Hurley, B.; Sabio, M.; Shen, X.; Gray, C.; Dzink-Fox, J.; Tao, J.; Cebula, R.; Wattanasin, S. Design and structure−activity relationships of potent and selective inhibitors of undecaprenyl pyrophosphate synthase (UPPS): tetramic, tetronic acids and dihydropyridin-2-ones. *Bioorg. Med. Chem. Lett.* **2008**, *18*, 1840−1844.
(60) Lindert, S.; Zhu, W.; Liu, Y.-L.; Pang, R.; Oldfield, E.; McCammon, J. A. Farnesyl Diphosphate Synthase Inhibitors from in Silico Screening. *Chem. Biol. Drug Des.* **2013**, *81*, 742−748.
(61) Jahnke, W.; Rondeau, J.-M.; Cotesta, S.; Marzinzik, A.; Pellé, X.; Geiser, M.; Strauss, A.; Götte, M.; Bitsch, F.; Hemmig, R.; Henry, C.; Lehmann, S.; Glickman, J. F.; Roddy, T. P.; Stout, S. J.; Green, J. R. Allosteric non-bisphosphonate FPPS inhibitors identified by fragment-based discovery. *Nature Chem. Biol.* **2010**, *6*, 660−666.
(62) Jahnke, W.; Henry, C. An in vitro Assay to Measure Targeted Drug Delivery to Bone Mineral. *ChemMedChem* **2010**, *5*, 770−776.

(63) Park, J.; Lin, Y.-S.; Tsantrizos, Y. S.; Berghuis, A. M. Ternary complex structures of human farnesyl pyrophosphate synthase bound with a novel inhibitor and secondary ligands provide insights into the molecular details of the enzyme's active site closure. *BMC Struct. Biol.* **2012**, *12*, 32.
(64) Räikkönen, J.; Taskinen, M.; Dunford, J. E.; Mönkkönen, H.; Auriola, S.; Mönkkönen, J. Correlation between time-dependent inhibition of human farnesyl pyrophosphate synthase and blockade of mevalonate pathway by nitrogen-containing bisphosphonate in cultured cells. *Biochem. Biophys Res. Commun.* **2011**, *407*, 663−667.
(65) Niesen, F. H.; Berglund, H.; Vedadi, M. The use of differential scanning fluorimetry to detect light interactions that promote protein stability. *Nature Protoc.* **2007**, *2*, 2212−2221.
(66) Otwinoski, Z, Minor, W. Processing of X-ray diffraction data collected in oscillation mode. In *Methods in Enzymology Macromolecular Crystallography Part A*; Charles, W. C., Ed.; Academic Press: New York, 1997; 307−326.
(67) Winter, G. *xia2*: an expert system for macromolecular crystallography data reduction. *J. Appl. Crystallogr.* **2010**, *43*, 186−190.
(68) Emsley, P.; Cowtan, K. Coot: model-building tools for molecular graphics. *Acta Crystallogr., Sect. D: Biol. Crystallogr.* **2004**, *60*, 2126−2132.
(69) Vagin, A. A.; Steiner, R. A.; Lebedev, A. A.; Potterton, L.; McNicholas, S.; Long, F.; Murshudov, G. N. REFMAC5 dictionary: organization of prior chemical knowledge and guidelines for its use. *Acta Crystallogr., Sect. D: Biol. Crystallogr.* **2004**, *60*, 2184−2195.
(70) Sparano, J. A.; Moulder, S.; Kazi, A.; Coppola, D.; Negassa, A.; Vahdat, L.; Li, T.; Pellegrino, C.; Fineberg, S.; Munster, P.; Malafa, M.; Lee, D.; Hoschander, S.; Hopkins, U.; Hershman, D.; Wright, J. J.; Kleer, C.; Merajver, S.; Sebti, S. M. Phase II Trial of Tipifarnib plus Neoadjuvant Doxorubicin-Cyclophosphamide in Patients with Clinical Stage IIB-IIC Breast Cancer. *Clin. Cancer Res.* **2009**, *15*, 2942−2948.
(71) (a) Yokoyama, K.; Zimmerman, K.; Scholten, J.; Gelb, M. H. Differential Prenyl Pyrophosphate Binding to Mammalian Protein Geranylgeranyltransferase-I and Protein Farnesyltransferase and Its Consequence on the Specificity of Protein Prenylation. *J. Biol. Chem.* **1997**, *272*, 3944−3952. (b) Rowinsky, E. K. Lately, It Occurs to Me What a Long, Strange Trip It's Been for the Farnesyltransferase Inhibitors. *J. Clin. Oncol.* **2006**, *24*, 2981.
(72) Zangi, R.; Hagen, M.; Berne, B. J. Effect of Ions on the Hydrophobic Interaction between Two Plates. *J. Am. Chem. Soc.* **2007**, *129*, 4678−4686.